

# Gas–liquid mass transfer in a novel forced circulation loop reactor

Ali Fadavi<sup>a,\*</sup>, Yusuf Chisti<sup>b</sup>

<sup>a</sup> Department of Farm Machinery, Faculty of Agricultural Engineering, Ilam University, P.O. Box 69315-516, Ilam, Iran

<sup>b</sup> Institute of Technology and Engineering, Massey University, Private Bag 11 222, Palmerston North, New Zealand

Received 18 March 2005; received in revised form 27 June 2005; accepted 29 June 2005

## Abstract

A forced circulation pumped loop reactor is characterized for oxygen transfer in air–water system. Overall mass transfer coefficient ( $k_La$ ) data are reported for airlift and forced circulation modes of operation, for liquid circulation rates of up to 2 m<sup>3</sup>/h. Highest values of oxygen transfer efficiency were attained at specific power input values of  $\leq 100$  W/m<sup>3</sup> when the forced circulation rates were  $\leq 0.5$  m<sup>3</sup>/h. Higher values of forced circulation rate reduced mass transfer efficiency, but reactor was always more efficient than a propeller loop reactor. The  $k_La$  values obtained at high rates of pumped liquid circulation were substantially greater than could be attained in the airlift mode of operation. Forced circulation produced more uniform and small bubbles, compared to operation as an airlift reactor. At high rates of forced circulation (e.g. 2 m<sup>3</sup>/h), presence of relatively light (density = 931.8 kg/m<sup>3</sup>) suspended hydrophobic polypropylene particles (average diameter = 4.7 mm) at concentrations of 1.6 and 3.2% (v/v), barely affected  $k_La$  compared to solids-free operation. The reactor used had an aspect ratio of 6.2 and downcomer-to-riser cross-sectional area ratio of 0.032. The forced flow was injected in the annular riser zone.

© 2005 Elsevier B.V. All rights reserved.

**Keywords:** Gas–liquid mass transfer; Oxygen transfer; Power consumption; Forced circulation loop reactor; Jet loop reactors; Airlift bioreactors

## 1. Introduction

Aerobic fermentations require an uninterrupted supply of dissolved oxygen. Oxygen is generally supplied by sparging air or pure oxygen through a pool of culture broth contained in a bioreactor. The oxygen absorption capability of a bioreactor is characterized in terms of the overall volumetric gas–liquid mass transfer coefficient, or  $k_La$ . The oxygen absorption rate  $N$  is related to  $k_La$  as follows [1]:

$$N = k_La(C^* - C_L) \quad (1)$$

where  $C^*$  is the saturation concentration of dissolved oxygen in the broth and  $C_L$  is the actual instantaneous concentration. Oxygen transfer capability of a bioreactor often limits its productivity and many bioreactor designs have been investigated in attempts to provide high levels of oxygen transfer at minimal power inputs [2].

In pneumatically mixed conventional bioreactors such as bubble columns, bubble flow persists only to a relatively low superficial aeration velocity of about 0.04 m/s [1,3]. Higher aeration rates increase bubble size, cause churn turbulent flow and lead to reduced mass transfer efficiency. Better oxygen transfer efficiencies than in bubble columns, have been reported for airlift reactors where bubble flow can occur to higher values of aeration velocities [1]. Various mechanisms for enhancing gas–liquid mass transfer in bioreactors have been reported. Low frequency vibrations applied to the liquid phase have been shown to reduce the size of gas bubbles generated at the sparger and enhance gas holdup and  $k_La$  by a factor of two or more [4]. Other methods of enhancing gas–liquid mass transfer in pneumatically mixed bioreactors include the use of static mixers [5–7], perforated plates [8] and baffles [9]. Installation of these internals has improved mass transfer by as much as 500% compared to when no internals are used [5]. Magnetic stabilization of slurries of suspended solids is a further option that is sometimes useful in enhancing mass transfer [10].

\* Corresponding author. Tel.: +98 841 2228059; fax: +98 841 2227015.  
E-mail address: a.fadavi@yahoo.com (A. Fadavi).

### Nomenclature

$a$	gas–liquid interfacial area per unit volume of liquid (1/m)
$C^*$	saturation concentration of dissolved oxygen (kmol/m <sup>3</sup> )
$C_L$	oxygen concentration in the liquid (kmol/m <sup>3</sup> )
$e_T$	total power input per unit volume (W/m <sup>3</sup> )
$E_M$	mass transfer efficiency (m <sup>3</sup> /J)
$g$	gravitational acceleration (m/s <sup>2</sup> )
$H_L$	unaerated liquid height (m)
$k_L$	mass transfer coefficient based on liquid film (m/s)
$k_{L,a}$	volumetric mass transfer coefficient (1/s)
$M$	molar mass (kg/kmol)
$N$	oxygen flux (kmol/m <sup>2</sup> s)
$P_{ts}$	pressure at top section (headspace) (Pa)
$\Delta P_s$	differential pressure between inlet and outlet of sparger (Pa)
$Q_g$	volumetric gas flow rate (m <sup>3</sup> /s)
$Q_L$	volumetric liquid flow rate (m <sup>3</sup> /h)
$Q_m$	molar gas flow rate (kmol/s)
$R$	universal gas constant (J/kmol K)
$T$	temperature (K)
$v_{LN}$	liquid velocity in nozzle (m/s)
$v_0$	gas velocity through the sparger hole (m/s)
$V_L$	liquid volume in the reactor (m <sup>3</sup> )
$V_{sgr}$	superficial gas velocity in riser (m/s)

### Greek symbols

$\varepsilon$	gas holdup
$\rho$	density (kg/m <sup>3</sup> )
$\Omega$	efficiency factor

### Subscript

D	dispersion
g	gas phase
L	liquid phase

When a microbial culture is not easily damaged by fluid shear, reactors such as jet loop bioreactor [11–13] and propeller loop reactor [14,15] can be used to achieve high rates of mixing and oxygen transfer. How gas is sparged in these reactors and the gas–liquid mixing in the “mixing tube” zones of spargers, influence oxygen transfer in these reactors [16–19]. Here we report on overall volumetric gas–liquid mass transfer coefficient in a novel forced circulation loop reactor for possible use as a bioreactor [20]. The reactor uses an external centrifugal pump to enhance liquid circulation in concentric draft-tube type of internal-loop airlift circulator. The intended applications span processes in which the biocatalyst is relatively shear-tolerant.

Various configurations of forced circulation loop reactors with externally located pumps have been described in the literature [11–13,16–19,21–28]. Generally, the pump is used to force a jet of liquid either upwards or downwards in a draft-tube that is concentrically located in an outer vessel. Fluid circulation between the draft-tube and the annular zone is driven by the momentum of the fluid jet. Jet loop reactors have been proposed mainly for use in chemical processes [27] and, to some extent, in biological treatment of wastewater. Compared to reactors such as the stirred tank, relatively few publications exist on jet loop reactors. Hydrodynamics [19,21,23–25,28], gas–liquid mass transfer [16–18,22,24], solid–liquid mass transfer [26] and mixing in these reactors have been studied. The forced circulation loop reactor of the present study was different from the other jet loop reactors that have been described. The entire annular zone of the reactor used in this work (Fig. 1) constituted an annular jet. Furthermore, the gas injection configuration used (Fig. 1) had been specifically designed to provide a high value of liquid flow rate parallel to the gas injection orifices, so that the bubbles detached from the sparger while they were still quite small. This increased gas–liquid interfacial area for mass transfer. The maximum flow in the inlet nozzle was about 7 m/s compared to a flow of about 20 m/s that is typical of jet loop reactors [11].

## 2. Materials and methods

### 2.1. Forced circulation loop reactor

The bioreactor consisted of a cylindrical vessel that was divided into riser and downcomer zones by insertion of a concentric draft-tube. The reactor vessel and gas–liquid sparger are shown in Fig. 1. The gas–liquid sparger (Fig. 1) consisted of separate inlets for gas and liquid. The liquid passed through a static mixer that induced a swirling motion. The gas from a side port was injected in the swirling liquid through annular holes (6 in Fig. 1) in the conical region of the gas sparger. The gas–liquid dispersion was intimately mixed in a mixing tube (8 in Fig. 1) and passed into the annular riser zone (riser) of the reactor. A guide cone placed at the bottom of the draft-tube ensured that the gas–liquid dispersion from the sparger smoothly flowed into the riser without disturbing the circulatory flow between the riser and the downcomer (draft-tube). Small gas bubbles were rapidly swept away from the injection holes by the rapid swirling flow of liquid. Size of the bubbles depended on the gas and liquid flow rates, as could be ascertained visually. A combination of high liquid flow rate and low gas flow rate produced small bubbles and good distribution of bubbles across the cross-section of the mixing tube. A typical uniform distribution of small bubbles in the annular riser zone is shown in Fig. 2. (The bubble concentration at the left and right edges of Fig. 2 appears higher than in the center because the camera is viewing a much deeper fluid channel at the edges of the reactor column than in the center.)

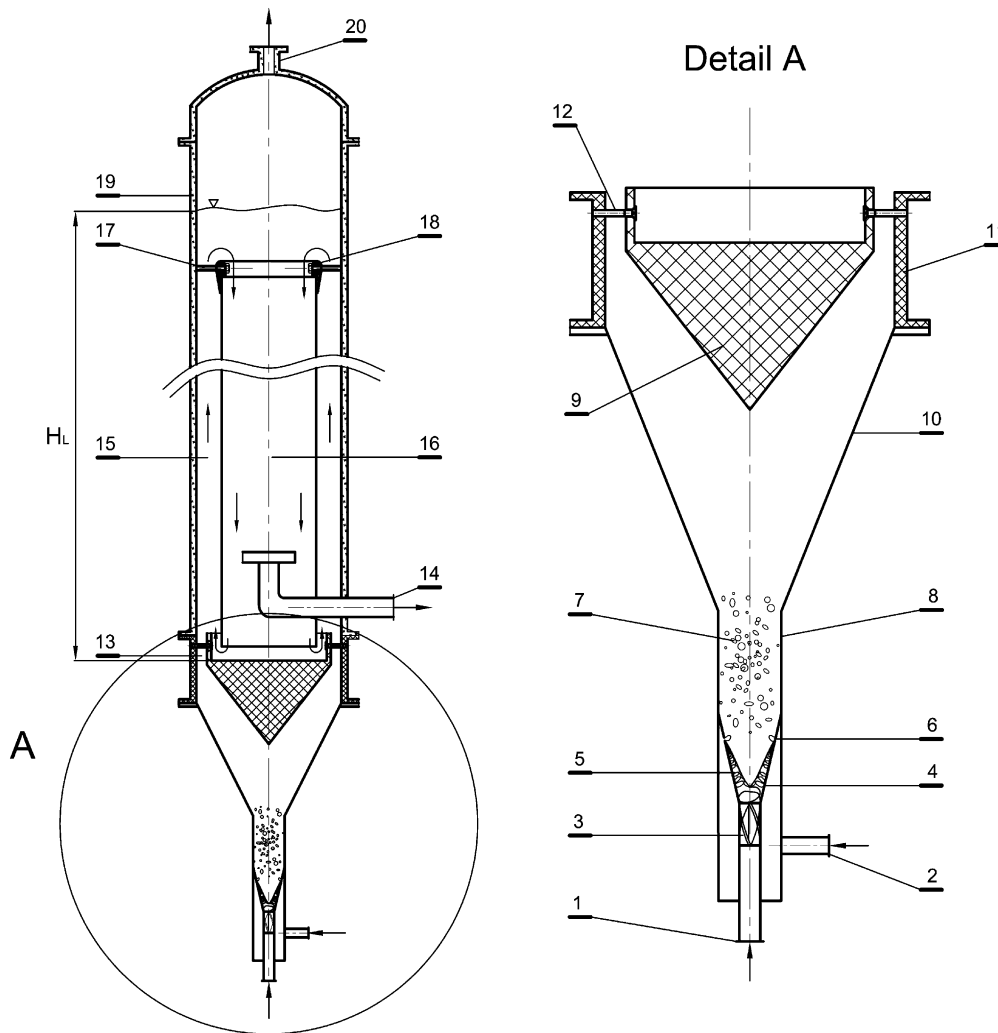


Fig. 1. Details of the reactor: (1) liquid inlet; (2) gas inlet; (3) static mixer; (4) gas sparger; (5) conical liquid input zone; (6) orifice; (7) two-phase mixture; (8) mixing tube; (9) guiding cone; (10) diffuser; (11) support; (12) screw; (13) riser venturi entrance; (14) liquid outlet; (15) riser; (16) downcomer; (17) screw; (18) draft-tube support; (19) reactor vessel; (20) gas outlet.



Fig. 2. A typical distribution of bubbles at  $Q_L = 2 \text{ m}^3/\text{h}$  and  $Q_g = 1.29 \times 10^{-4} \text{ m}^3/\text{s}$ .

Table 1  
Reactor geometry and operational parameters

Description	Value
Bioreactor diameter (m)	0.1484
Un aerated liquid height (m)	0.914
Liquid height above draft-tube (m)	0.032
Working volume (m <sup>3</sup> )	0.01625
Downcomer-to-riser cross-section area ratio (–)	0.493
Draft-tube length (m)	0.865
Inner diameter of draft-tube (m)	0.083
Static mixer S <sub>1</sub>	20 mm length, 45° inclination angle
Static mixer S <sub>2</sub>	20 mm length, 90° inclination angle
Mixing tube length (m)	0.124 and 0.236

The circulation of liquid in the riser–downcomer loop was higher than would be the case in an equivalent airlift reactor because the circulation was driven by the external centrifugal pump that was in addition to the driving force contributed by the difference in density of dispersion between the riser and downcomer.

Various geometric details of the reactor are shown in Table 1. The arrangement of gas and liquid flow, pressure measurement points and the location of dissolved oxygen sensors are shown in Fig. 3. All experiments were carried out with air and water at  $20 \pm 1$  °C. The temperature of the liquid in the reactor was controlled by passing the liquid flow from the pump through a cooler before the liquid entered the reactor. Air was sourced from a laboratory compressor via a pressure regulator, needle valve and a buffer tank that facilitated precise adjustments of gas flow rate. Some experiments used solid particles suspended in water. The solid phase consisted of polypropylene particles of 4.7 mm mean diameter and 931.8 kg/m<sup>3</sup> density, respectively.

## 2.2. Measurements

Overall gas holdup,  $\varepsilon$ , was determined by the well-known volume expansion method [1]. This method is reproducible to within  $\pm 10\%$  of the average value [1]. The overall volumetric mass transfer coefficient,  $k_L a$ , was determined by means of the dynamic gassing-out method [1]. Two different makes of dissolved oxygen probes (Jenway 9300, UK; WTW 537, Germany) were used. The  $k_L a$  data obtained by these probes agreed within  $\pm 7.6\%$  of the average value, for a range of identical conditions of comparison. The probes were located as shown in Fig. 3. The probe in the draft-tube was at the centerline, 0.31 m below the top of the vessel. Both probes were approximately half way up the reactor. The probe in the riser zone extended to the mid point of the annulus and was inclined at 17° to the horizontal (Fig. 3).

For  $k_L a$  measurements, dissolved oxygen was first removed from the reactor by sparging with nitrogen until the dissolved oxygen concentration fell to nearly zero. The

nitrogen flow was then stopped and bubbles were allowed to disengage from the liquid. Aeration commenced and the flow rate of air was adjusted to the required value. The air flow rate was calculated based on the hydrostatic pressure at the entrance of the gas sparger. Once the reactor had attained a hydrodynamic steady state by visual inspection (typically <20 s from initiation of aeration), the increase in dissolved oxygen concentration was measured with time until the fluid became nearly saturated with oxygen. Output signals from the dissolved oxygen meters were logged using an IBM compatible computer, at intervals of 1 or 2 s. The response times of the dissolved oxygen electrodes ( $\sim 6$  s for 63% of full scale response) was always  $\leq 1/k_L a$  and therefore electrode response delays could be neglected in calculations of  $k_L a$  [15].

Dissolved oxygen concentrations measured as a function of time, were used in calculating the  $k_L a$ . Data collected only after the first 20 s of start of aeration were used. For the conditions used, the increase in dissolved oxygen with time is described by the following well-known equation [1]:

$$\frac{dC_L}{dt} = k_L a (C^* - C_L) \quad (2)$$

Integration of Eq. (2) for  $C_L = C_0$  at  $t = 0$ , led to the following equation:

$$\ln \left( \frac{C^* - C_L}{C^* - C_0} \right) = -k_L a t \quad (3)$$

A plot of the left-hand-side of Eq. (3) against time, was used to obtain the slope as  $-k_L a$ .

Measurements of pressure difference  $\Delta P$  at the inlet and outlet of the sparging zone (Fig. 3) for estimating the energy consumption were done with a differential pressure transmitter (Rosemount 3051, USA). Differential pressure signals were transmitted and logged on a computer at 1 s intervals within a measurement window of 30 s. The total power input  $e_T$  to the reactor was estimated as follows:

$$e_T = \frac{Q_m R T}{V_L} \ln \left( 1 + \frac{\rho_L g H_L}{P_{ts}} \right) + \frac{\Omega}{2V_L} Q_m M v_o^2 + \frac{Q_L}{2V_L} \rho_L v_{LN}^2 + \frac{\Delta P_s Q_L}{V_L} \quad (4)$$

The first, second, third and fourth terms on the right-hand-side of Eq. (4) represented power input due to isothermal expansion of the gas, the kinetic energy of the injected gas, the kinetic energy of the liquid entering the reactor, and the energy loss in the sparger zone. The efficiency factor  $\Omega$  was taken to be 1 [1]. Derivation of the first two terms of Eq. (4) has been discussed in detail previously [1]. Terms three and four in the above equation have been commonly derived in textbooks dealing with fluid flow in pipes [29].

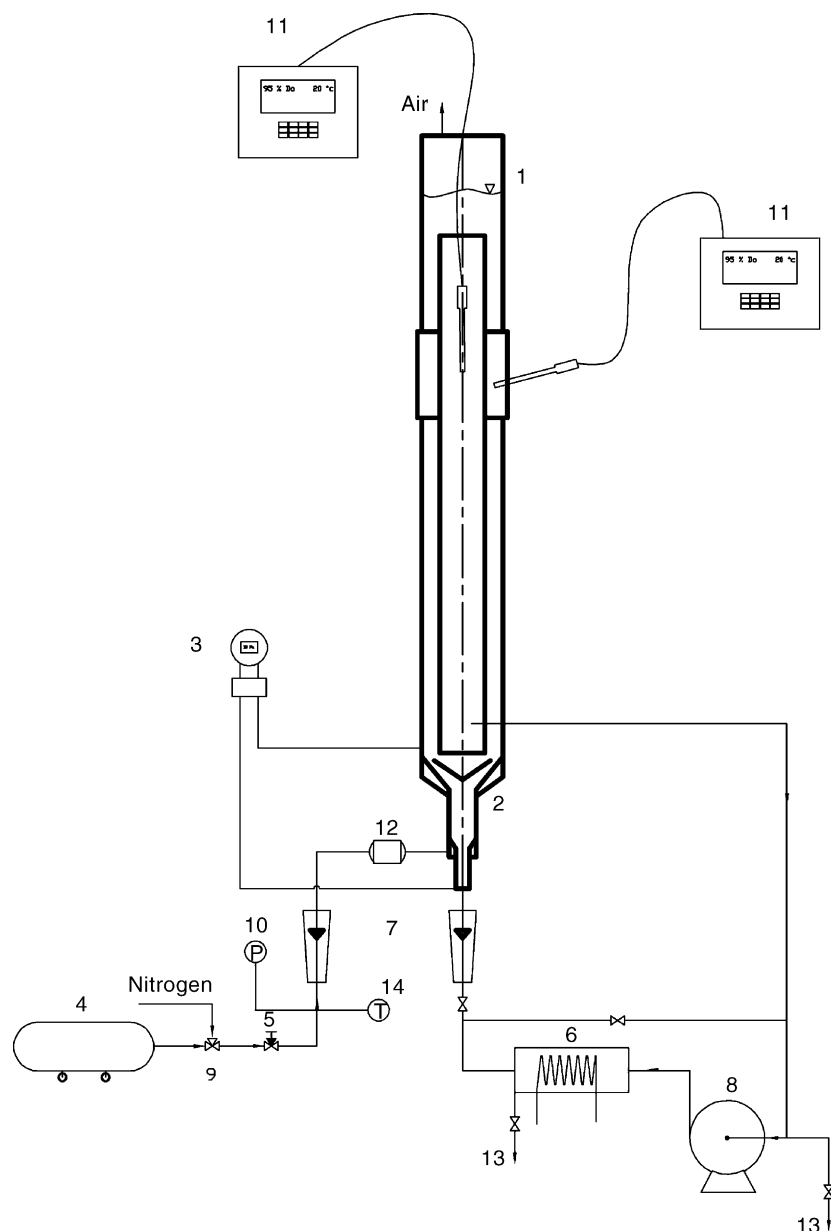


Fig. 3. Forced circulation loop reactor and ancillary equipment. (1) Reactor; (2) gas–liquid sparger; (3) differential pressure transmitter; (4) compressor; (5) needle valve; (6) cooler; (7) rotameter; (8) centrifugal pump; (9) three-way valve; (10) pressure gage; (11) dissolved oxygen meter; (12) buffer tank; (13) drain valve; (14) thermometer.

### 3. Result and discussion

#### 3.1. Mass transfer

Dependence of the overall gas holdup and  $k_L a$  on the main operational variables of liquid flow rate and aeration rate, is shown in Figs. 4 and 5, respectively. Both gas holdup and  $k_L a$  values were enhanced by increasing gas and liquid flow rates. Compared to operation as an airlift (i.e.  $Q_L = 0$ ), use of pumped circulation enhanced  $k_L a$  by nearly two-fold at a  $Q_L$  value of  $2 \text{ m}^3/\text{h}$  (Fig. 5). A similar behavior was seen for

gas holdup (Fig. 4). Therefore, the liquid flow influenced  $k_L a$  mainly by affecting the bubble size and gas–liquid interfacial area  $a$ .

The  $k_L a$  values obtained generally depended on the total power input in the reactor, as shown in Fig. 6 for various values of the pumped liquid flow. For relatively low pumping rates ( $0 \leq Q_L \leq 1 \text{ m}^3/\text{h}$ ), the turbulence was low and the flow contributed little to breaking gas bubbles; hence, for  $Q_L \leq 1 \text{ m}^3/\text{h}$ , the  $k_L a$  values were essentially the same as for the conventional airlift mode of operation (i.e.  $Q_L = 0$ ) (Fig. 6). For solids-free and forced operations, the  $k_L a$

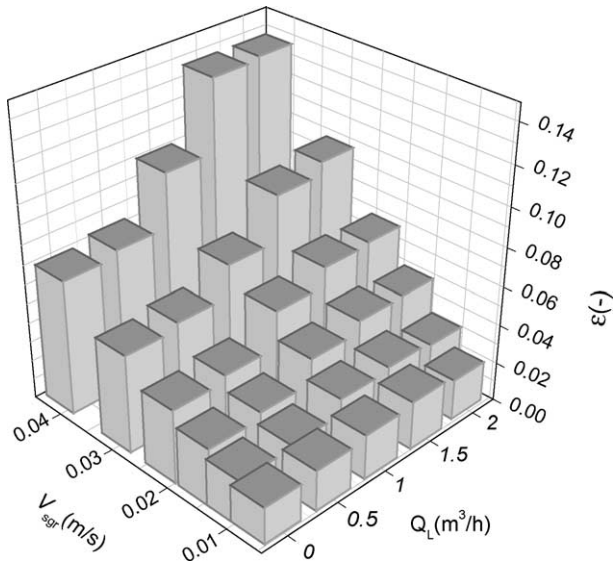


Fig. 4. Overall gas holdups ( $\epsilon$ ) vs. superficial gas velocity ( $V_{sgr}$ ) for different liquid flow rates ( $Q_L$ ).

data were correlated with the power input and gas holdup, according to the following equation:

$$k_L a = 19.91 \times 10^{-3} e_T^{0.361} \epsilon^{0.667} \quad (5)$$

Predictions of Eq. (5) agreed with the measured  $k_L a$  values to within  $\pm 6.9\%$  average deviation. The maximum deviation was within  $\pm 15\%$  (Fig. 7).

The method used for calculating the  $k_L a$  assumed a well-mixed liquid phase. This assumption is supported by the data shown in Fig. 8 where, for any combination of gas and liquid flow rates, the measured  $k_L a$  values in the riser and downcomer zones agreed on average within 5%. For any given pumping rate of liquid, the  $k_L a$  values increased with increasing aeration rate because of increasing gas holdup

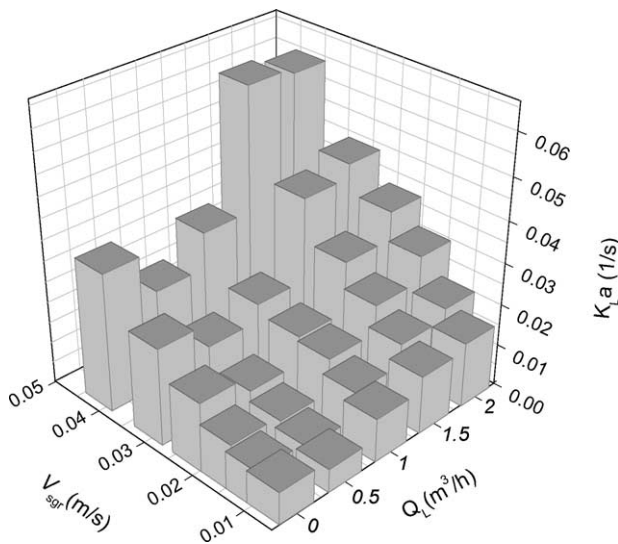


Fig. 5. Overall mass transfer coefficient ( $k_L a$ ) vs. superficial gas velocity ( $V_{sgr}$ ) for different liquid flow rates ( $Q_L$ ).

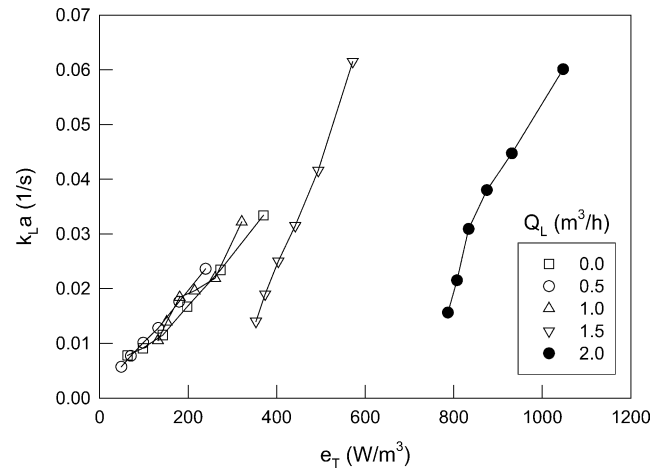


Fig. 6. Volumetric mass transfer coefficient ( $k_L a$ ) vs. volumetric power input ( $e_T$ ).

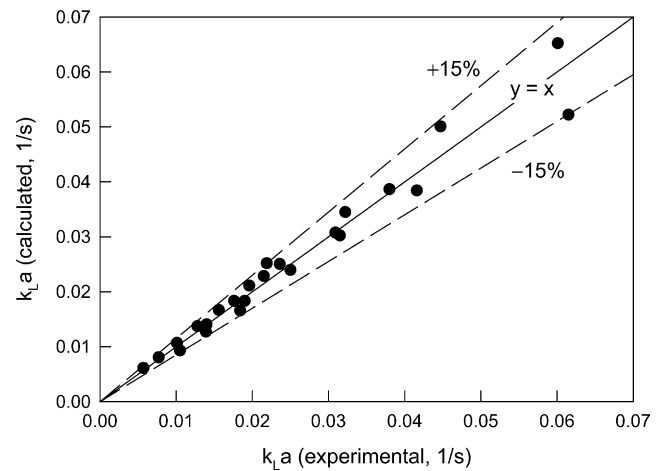


Fig. 7. Comparison of the predictions of Eq. (5) with measured values of the volumetric mass transfer coefficient.

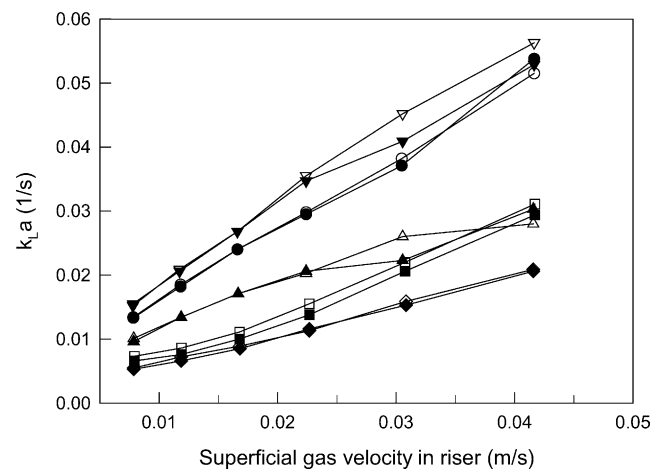


Fig. 8. Mass transfer coefficient ( $k_L a$ ) vs. superficial gas velocity in riser (hollow symbols) and downcomer (solid symbols) at different liquid flow rate ( $m^3/h$ ): 0 ( $\square$ ), 0.5 ( $\diamond$ ), 1.0 ( $\triangle$ ), 1.5 ( $\circ$ ) and 2.0 ( $\nabla$ ).

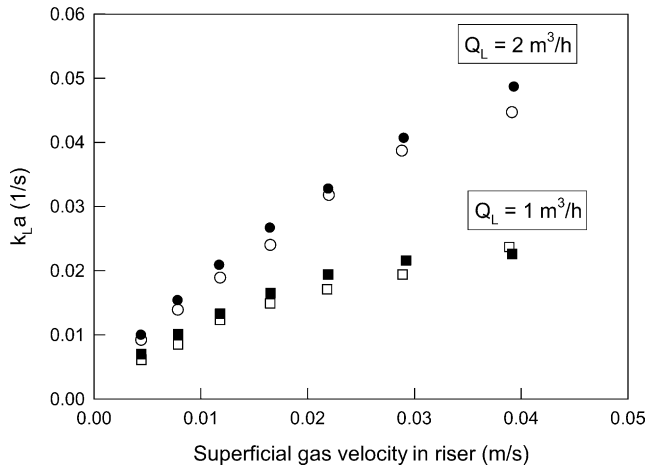


Fig. 9. Overall mass transfer coefficient vs. superficial gas velocity for liquid flow rate ( $Q_L$ ) values of 1 and 2  $\text{m}^3/\text{h}$  and two different static mixers  $S_1$  (solid symbols) and  $S_2$  (hollow symbols).

and interfacial area (Fig. 8). For any fixed aeration rate,  $k_La$  increased with increasing liquid flow rate because the turbulence generated by the liquid reduced the size of gas bubbles and increased interfacial area. Increasing liquid flow was increasingly effective in dispersing bubbles at higher values of aeration rate (Fig. 8). This is because bubble coalescence becomes an important factor in reducing interfacial area only at relatively high values of aeration velocity.

The  $k_La$  values were comparable for the two static mixers (Fig. 9), suggesting that the lower pressure drop mixer  $S_1$  is to be preferred. For any given static mixer, the flow rate of the liquid had a strong influence on the  $k_La$  (Fig. 9), as explained earlier. An approximate doubling of the length of the mixing tube in the sparger zone (Fig. 1) did not affect the  $k_La$  values substantially, but the  $k_La$  values were strongly influenced by the volume flow rate of liquid through the mixing tube (Fig. 10). Compared to a volumetric liquid flow rate of 1  $\text{m}^3/\text{h}$ , a doubling of the flow increased turbulence, produced

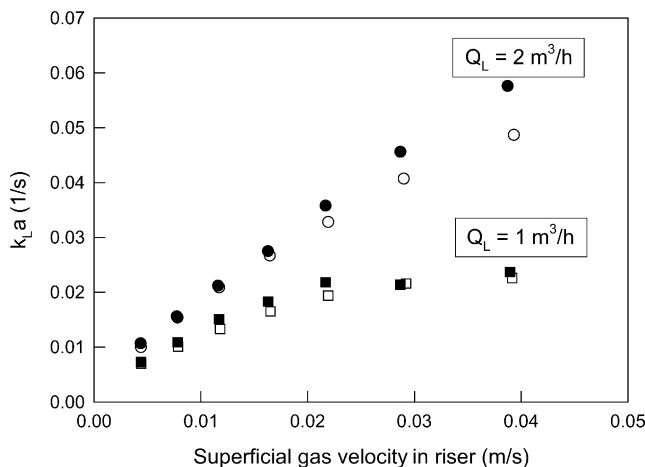


Fig. 10. Overall mass transfer coefficient ( $k_La$ ) vs. superficial gas velocity for different mixing tube lengths (solid symbols = long tube; hollow symbols = short tube) and liquid flow rates  $Q_L$ .

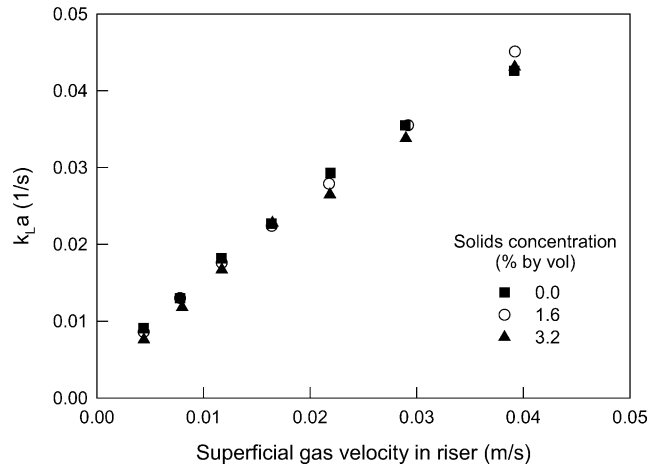


Fig. 11. Overall mass transfer coefficient ( $k_La$ ) values for different solids loadings at  $Q_L = 2 \text{ m}^3/\text{h}$ .

finer bubbles and distributed the bubbles more uniformly across the cross-section of the tube, to greatly enhance the  $k_La$  (Fig. 10).

Presence of ridged polypropylene particles in the liquid at concentrations of up to 3.2 vol.% solids had barely any effect on  $k_La$  (Fig. 11) compared to equivalent two-phase operation. The effect of solids was assessed only at the high liquid pumping rate of 2  $\text{m}^3/\text{h}$ . In airlift reactors, presence of pulp-like solids at similar concentrations as used here, is known to reduce the  $k_La$  values significantly compared to solids-free operation [1]. Thus, the effect of solids depends on the kind of solids. Certain types of relatively large and heavy solid particles suspended in low concentrations can actually increase the value of  $k_La$  [30]. This is apparently caused by the solids reducing the bubble size and thereby increasing the gas–liquid interfacial area.

### 3.2. Mass transfer efficiency

Mass transfer efficiency  $E_m$  is defined [15] as follows:

$$E_m = \frac{k_La}{e_T} \quad (6)$$

Multiplying the  $E_m$ -value with the steady-state driving force for oxygen transfer (i.e.  $C^* - C_L$ ), provides the amount of oxygen transferred per unit of energy supplied. Mass transfer efficiencies for various levels of power input are shown in Fig. 12. Published data [15] for a propeller loop reactor are also shown for comparison. Highest values of oxygen transfer efficiency were attained at specific power input values of  $\leq 100 \text{ W}/\text{m}^3$  when the forced circulation rates were  $\leq 0.5 \text{ m}^3/\text{h}$ . High values of forced circulation rate reduced mass transfer efficiency; nevertheless, for the entire range of  $Q_L$  values tested, the forced circulation operation was more efficient in comparison with a propeller loop reactor that has been reported in the literature [15]. Centrifugal pump is clearly a more efficient circulator than a conventional propeller located within a tube.

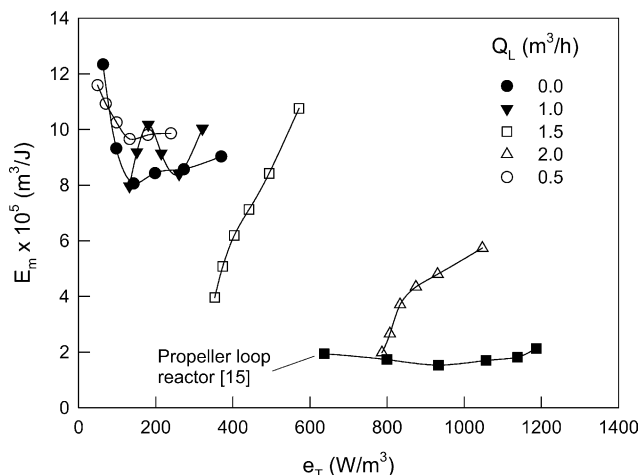


Fig. 12. Comparison of mass transfer efficiency  $E_m$  at different liquid flow rates in the forced circulation loop reactor with values reported for the propeller loop reactor [15].

#### 4. Conclusions

Gas–liquid mass transfer was characterized in a pumped circulation loop reactor for various combinations of aeration rates and pumped flow rates of liquid. Compared to operation as airlift circulator (i.e. no external pumping), forced circulation greatly enhanced  $k_L a$  and gas holdup particularly when the pumped liquid flow exceeded  $1 \text{ m}^3/\text{h}$ . The  $k_L a$  enhancing effect of forced liquid circulation was particularly strong at high aeration rates when bubble coalescence would have adversely affected  $k_L a$  in the absence of forced flow of liquid. The measured  $k_L a$  correlated with total power input and gas holdup in the reactor. Ridged, relatively light, hydrophobic suspended solids did not significantly affect  $k_L a$  at solids concentration of up to 3.2% by volume. Highest values of oxygen transfer efficiency were attained at specific power input values of  $\leq 100 \text{ W/m}^3$  when the forced circulation rates were  $\leq 0.5 \text{ m}^3/\text{h}$ . Compared to published data on a propeller driven loop reactor [15], the oxygen transfer efficiency of the pumped circulation reactor was significantly higher.

#### References

- [1] M.Y. Chisti, *Airlift Bioreactors*, Elsevier, London, 1989.
- [2] Y. Chisti, Mass transfer, in: M.C. Flickinger, S.W. Drew (Eds.), *Encyclopedia of Bioprocess Technology: Fermentation, Biocatalysis, and Bioseparation*, vol. 3, Wiley, New York, 1999, pp. 1607–1640.
- [3] Y.T. Shah, B.G. Kelkar, S.P. Godbole, W.D. Deckwer, Design parameters estimations for bubble column reactors, *AIChE J.* 28 (1982) 353–379.
- [4] J. Ellenberger, R. Krishna, Shaken, not stirred, bubble column reactors: enhancement of mass transfer by vibration excitement, *Chem. Eng. Sci.* 58 (2003) 705–710.
- [5] Y. Chisti, M. Kasper, M. Moo-Young, Mass transfer in external-loop airlift bioreactors using static mixers, *Can. J. Chem. Eng.* 68 (1990) 45–50.
- [6] C.U. Ugwu, J.C. Ogbonna, H. Tanaka, Improvement of mass transfer characteristics and productivities of inclined tubular photobioreactors by installation of internal static mixers, *Appl. Microbiol. Biotechnol.* 58 (2002) 600–607.
- [7] M. Gavrilescu, R.V. Roman, R.Z. Tudors, Hydrodynamics in external-loop airlift bioreactors with static mixers, *Bioproc. Eng.* 16 (1997) 93–99.
- [8] S. Krichnavaruk, P. Pavasant, Analysis of gas–liquid mass transfer in an airlift contactor with perforated plate, *Chem. Eng. J.* 89 (2002) 203–211.
- [9] T. Vorapongsathorn, P. Wongsuchoto, P. Pavasant, Performance of airlift contactors with baffles, *Chem. Eng. J.* 84 (2001) 551–556.
- [10] Z. Al-Qodah, M. Al-Hassan, Phase holdup and gas-to-liquid mass transfer coefficient in magneto stabilized G–L–S airlift fermenter, *Chem. Eng. J.* 79 (2000) 41–52.
- [11] H. Blenke, Loop reactors, *Adv. Biochem. Eng.* 13 (1979) 120–214.
- [12] U. Wachsmann, N. Rübiger, A. Vogelpohl, The compact reactor—a newly developed loop reactor with a high mass transfer performance, *Ger. Chem. Eng.* 7 (1984) 39–44.
- [13] U. Wachsmann, N. Rübiger, A. Vogelpohl, Effect geometry on hydrodynamics and mass transfer in compact reactor, *Ger. Chem. Eng.* 8 (1985) 411–418.
- [14] M.D.J. Pollard, A.P. Ison, P. Ayazi Shamlou, M.D. Lilly, Influence of a propeller on *Saccharomyces cerevisiae* fermentations in a pilot scale airlift bioreactor, *Bioproc. Eng.* 16 (1997) 273–281.
- [15] Y. Chisti, U.J. Jauregui-Haza, Oxygen transfer and mixing in mechanically agitated airlift bioreactors, *Biochem. Eng. J.* 10 (2002) 143–153.
- [16] C.A.M.C. Dirix, K. Van der Wiele, Mass transfer in jet loop reactors, *Chem. Eng. Sci.* 45 (1990) 2333–2340.
- [17] G.M. de Billerbeck, J.S. Condoret, C. Fonade, Study of mass transfer in a novel gas–liquid contactor: the aero-ejector, *Chem. Eng. J.* 72 (1999) 185–193.
- [18] P.H.M.R. Cramers, A.A.C.M. Beenackers, Influence of the ejector configuration, scale and the gas density on the mass transfer characteristics of gas–liquid ejectors, *Chem. Eng. J.* 82 (2001) 131–141.
- [19] P. Havelka, V. Linek, J. Sinkule, J. Zahradnik, M. Fialova, Effect of the ejector configuration on the gas suction rate and gas hold-up in ejector loop reactors, *Chem. Eng. Sci.* 52 (1997) 1701–1713.
- [20] A. Fadavi, Circulation reactor, Patent Application SK4135U, Industrial Property Office of Slovak Republic, 2004.
- [21] S.R. Bhutada, V.G. Pangarkar, Gas induction and hold-up characteristics of liquid jet loop reactors, *Chem. Eng. Commun.* 61 (1987) 239–258.
- [22] H.J. Warnecke, P. Hussmann, Volumetric mass transfer coefficients of gas–liquid jet loop reactors by oxidation of hydrazine, *Chem. Eng. Commun.* 78 (1989) 131–138.
- [23] L. Thorslund, M.H. Jorgensen, Characterisation of liquid and gas flow in jet loop reactors, *Bioproc. Eng.* 19 (1998) 129–136.
- [24] P. Havelka, V. Linek, J. Sinkule, J. Zahradnik, M. Fialova, Hydrodynamic and mass transfer characteristics of ejector loop reactors, *Chem. Eng. Sci.* 55 (2000) 535–549.
- [25] P. Mier, M. Kraume, Operating behaviour and scale-up of jet loop reactors in single phase operation, *Chem. Ing. Technol.* 72 (2000) 463–467 (in German).
- [26] J.P. Wen, L. Huang, Y. Zhu, C. Li, Y.L. Chen, Solid-liquid mass transfer in a gas–liquid–solid three-phase reversed flow jet loop reactor, *Chem. Eng. J.* 78 (2000) 231–235.
- [27] E.H. Stitt, Alternative multiphase reactors for fine chemicals—a world beyond stirred tanks? *Chem. Eng. J.* 90 (2002) 47–60.
- [28] J.T. Tinge, A.J.R. Casado, Influence of pressure on the gas hold-up of aqueous activated carbon slurries in a down flow jet loop reactor, *Chem. Eng. Sci.* 57 (2002) 3575–3580.
- [29] J.M. Coulson, J.F. Richardson, J.R. Backhurst, J.H. Harker, *Chemical Engineering*, vol. 1, 4th ed., Pergamon, Oxford, 1990.
- [30] Jianping Wen, Ping Na, Lin Huang, Yunlin Chen, Local overall volumetric gas liquid mass transfer coefficients in gas–liquid–solid reversed flow jet loop bioreactor with a non-Newtonian fluid, *Biochem. Eng. J.* 5 (2000) 225–229.